Journal of Magnetism and Magnetic Materials 536 (2021) 168067

Contents lists available at ScienceDirect

Journal of Magnetism and Magnetic Materials

journal homepage: www.elsevier.com/locate/jmmm

Research articles

Comparison of 3-D and 2-D models of a soft magnetic composite material

Joonas Vesa [1,*], Paavo Rasilo

Unit of Electrical Engineering, Tampere University, Tampere 33720, Finland

ARTICLE INFO

Keywords:
B-H curve
Geometry generation
Magnetic contact
Material identification
Soft magnetic composite
Voronoi tessellation

ABSTRACT

In this article, we compare 3-D finite element models of a soft magnetic composite (SMC) material to 2-D models, obtained by slicing some 2-D intersections of the 3-D geometries, in terms of magnetization curves and losses. A 3-D nonlinear static model, providing computational *B-H* curves, is compared to two 2-D models, one with the magnetic field parallel to the 2-D plane, and the other with the magnetic field perpendicular to the 2-D plane. We find that the 2-D models provide largely inconsistent results with the 3-D model. A 3-D time-harmonic model, providing computational effective permeabilities and losses, is compared to two 2-D models, one with the magnetic field parallel to the 2-D plane, and the other with the magnetic field perpendicular to the 2-D plane. We find that the 2-D models provide largely inconsistent results with the 3-D model, with an exception of the computational losses of the 2-D model, with the magnetic field perpendicular to the plane, almost agreeing with the computational losses provided by the 3-D model. However, the computational permeabilities do not match in these two models. This article proposes to be very critical before publishing 2-D models of SMC materials without a proper justification by symmetry.

1. Introduction

Soft magnetic composite (SMC) materials consist of ferromagnetic particles coated with an insulation, compressed and heat treated. Due to the special structure the materials have, eddy current losses are reduced. SMCs may be tailored so that the electromagnetic behaviour of the material is isotropic in the macroscale [1]. In Fig. 1a, we see a microscope image of an SMC material.

Various models of SMC materials have been presented in the past. Many of the models are based on meshing a 2-D geometry and computing the desired electromagnetic quantities using some finite element (FE) formulation [2–11]. Some of the cited articles do not claim the 2-D models to represent any existing material, but are test benches for the methods. However, the question about the applicability of 2-D models of SMC materials has been raised in the literature, since usually there is no symmetry that justifies such computations [4,8].

The question if 2-D and 3-D models provide consistent results for nonlinear *B-H* curves has been addressed in the literature [12]. However, a comprehensive comparison of 2-D and 3-D models is still missing. In this article, we give evidence that 2-D models of SMC materials are mostly inconsistent with 3-D models. The methods used are based on our approach of generating 3-D imitations of SMC materials [13–15]. In Fig. 1b we see one such geometry.

2. Measurements

Our sample is an MPP toroid C055106A2 by Magnetics Inc. [16]. We used a two-coil setup to measure the magnetic flux density (B) and field strength (H) waveforms in the material. A large-signal measurement with a 50-Hz excitation was carried out. The hysteresis loop obtained has been visualized in Fig. 4. Hysteresis seems to be very negligible.

A small-signal dynamical frequency sweep with a frequency range of 1 kHz – 20 kHz was carried out while keeping the peak flux density at 0.05 T. The waveforms of B and H were sinusoidal. The measured dynamical effective permeability is visualized in Fig. 8 and the measured losses are visualized in Fig. 9. The dynamical measurement is essentially the same as in our previous article [15].

3. Geometries

We define two sets of randomized geometries. First, we define 3-D geometries, and then we define 2-D geometries as sliced intersections of 3-D geometries.

* Corresponding author.
E-mail address: joonas.vesa@tuni.fi (J. Vesa).
[1] https://tutcris.tut.fi/portal/en/persons/joonas-vesa(c7791107-71f3-413e-a85e-f8b4b7424509).html

https://doi.org/10.1016/j.jmmm.2021.168067
Received 15 December 2020; Received in revised form 8 March 2021; Accepted 28 April 2021
Available online 13 May 2021

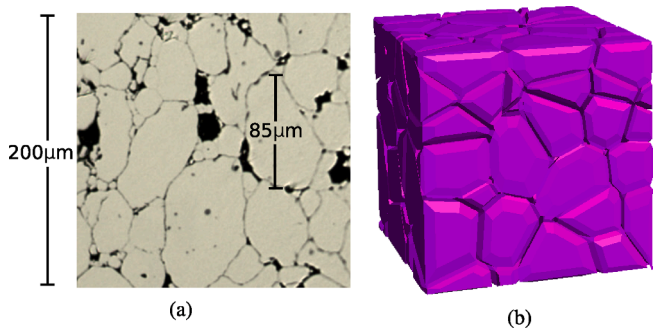

Fig. 1. (a) A microscope image of a Fe-Ni-Mo alloy SMC [16]. (b) A generated imitation of an SMC material geometry.

3.1. 3-D geometries

Based on the parameters shown in Table 1, we place a number N of points randomly into the cube $[0,1]^3$ under the condition that the points must be at least a distance d away from one another. A Voronoi tessellation is calculated based on the randomly placed points. The cell faces are refined based on the data in the vector w_F, and the cell faces are moved inside the cells according to the data in the vector w_C to form gaps between the particles. A total of 200 geometries were generated. One such geometry is visualized in Fig. 1b. A detailed description of the geometries has been presented earlier in [13].

We note that at first, the generated geometries are such that the neighbouring particles are in contact with each other. This is not desired, since the idea of SMC materials is to provide insulations between the particles. Hence, the contact surfaces are treated later in the computational methods as thin insulations by doubling the degrees of freedom of the contact surfaces and connecting the doubled degrees of freedom by thin prism elements in 3-D.

3.2. 2-D geometries

A total of 200 3-D geometries were generated based on the same parameters, shown in Table 1, and from each, one cross-sectional slice was extracted. An image of one such 2-D geometry can be found in Fig. 2. Similarly to the 3-D geometries, the insulations of the 2-D geometries are modeled by doubling the degrees of freedom of the contact regions in the FE mesh and connecting the degrees of freedom by thin rectangular elements.

4. Nonlinear models

In this section, we compare three problems that use the same nonlinear material model. We compare a magnetostatic 3-D problem with two magnetostatic 2-D problems, one with the field parallel to the plane and the other with the field perpendicular to the plane.

4.1. Magnetostatic 3-D problem

Consider a 3-D geometry, for instance the one depicted in Fig. 1b. The geometry is much like the simplified drawing in Fig. 3. The cube is scaled so that its side length is $l = 5{\cdot}85\ \mu\text{m} = 425\ \mu\text{m}$. The scaling is taken from Fig. 1a, where the diameter of one particle is approximately

Table 1
Geometry template

N	$5^3 = 125$
d	0.45/5
w_F	[0,0.4]
w_C	[0.1,0]

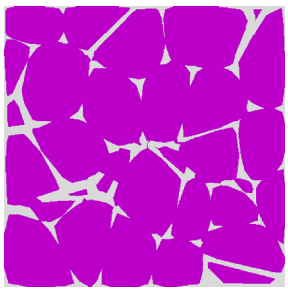

Fig. 2. A 2-D cross section of a 3-D geometry.

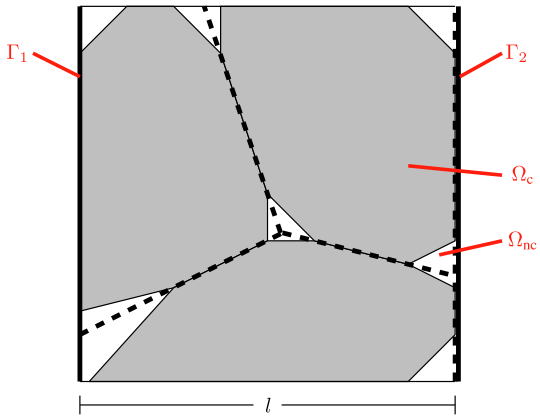

Fig. 3. A simplification of the geometries.

85 μm. Since there are $5^3 = 125$ particles in one cube, the side is scaled to $5{\cdot}85\ \mu\text{m} = 425\ \mu\text{m}$. The magnetizing particles, denoted by Ω_c, are meshed with tetrahedra. The thick parts of the empty regions Ω_{nc} are meshed with tetrahedra as well, and the thin insulations, denoted by the dashed lines in Fig. 3, are modeled with 42.5 nm thick prisms. The thickness of the insulations cannot be reliably measured from the microscope image presented in Fig. 1a, but according to Vesa et al., this thickness provides consistent results with measured losses and measured permeabilities [15].

In the domain $\Omega = \Omega_c \cup \Omega_{nc}$ it holds that

$$\nabla{\cdot}\mathbf{B}(\nabla\varphi) = 0 \tag{1}$$

for a magnetic scalar potential φ. The relation $\mathbf{B}(\cdot)$ is just a multiplication by the vacuum permeability μ_0 in Ω_{nc} and a nonlinear relation in Ω_c. The nonlinear part is given by an isotropic extension of the scalar relation, the 'Estimated local' curve, depicted in Fig. 4a. The curve was found by performing an estimation, described in [13].

Eq. (1) is discretized by the Galerkin method using a first order nodal scalar basis. On Γ_1, we set $\varphi = 0$, and on Γ_2, we set $\varphi = H_{\text{eff}} l$, which corresponds to the magnetomotive force between Γ_2 and Γ_1. The quantity H_{eff} is called an effective magnetic field strength. An effective magnetic flux density is given by

$$B_{\text{eff}} = \frac{1}{\text{Vol}} \int_\Omega \mathbf{B}{\cdot}\mathbf{e}_1, \tag{2}$$

where the unit vector $\mathbf{e}_1$ is perpendicular to Γ_1 and Γ_2.

The effective B-H curves of the 200 3-D models were computed and the computational results are depicted in Fig. 4a as 'Computed, 3-D'. The agreement between the computed curves and the measured curve is excellent since the localized B-H relation, denoted as 'Estimated local', for the magnetizing particles has been estimated by fitting one of the computational curves against the measurement data. A visualization of a computational B field can be found in Fig. 5a.

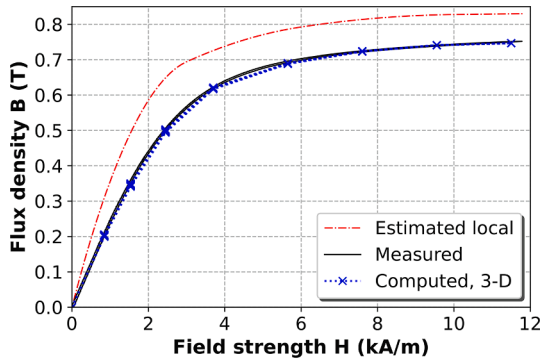

(a)

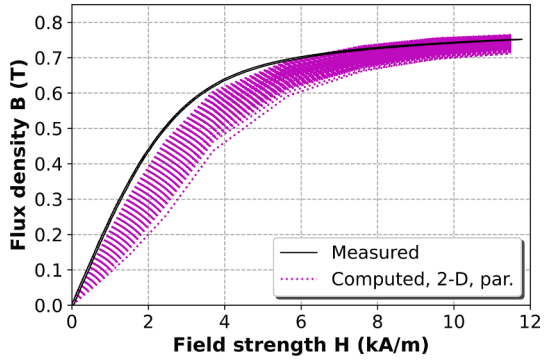

(b)

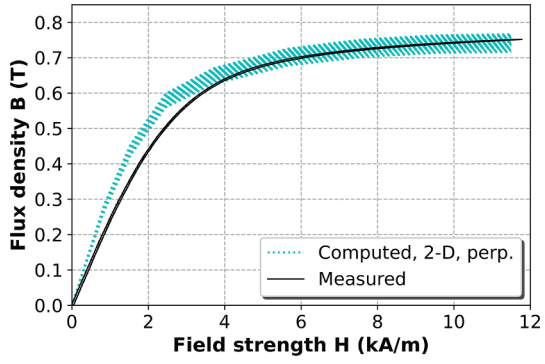

(c)

Fig. 4. Nonlinear static *B-H* curves. A comparison of 3-D and 2-D models.

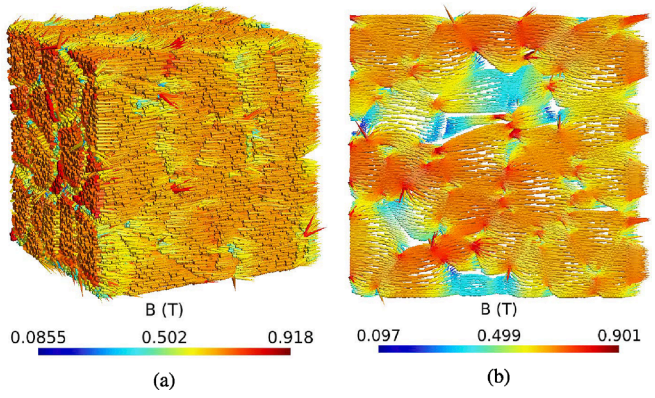

(a) (b)

Fig. 5. *B*-fields of a nonlinear 3-D model and a nonlinear 2-D model with the field parallel to the plane. The *H*-excitation was 3.7 kA/m in both cases.

4.2. Magnetostatic 2-D problem, field parallel to the plane

Consider the geometry in Fig. 2. We assume the magnetic field to traverse from the left edge to the right edge of the geometry on the plane. The Eqs. (1) and (2), as well as the constitutive model and the boundary conditions used in the 3-D model in Section 4.1 are still valid in 2-D (but not justified by any symmetry). The thin insulations, depicted in Fig. 3, are modeled with thin quadrangles in the 2-D case. The thicknesses of the quadrangles, however, are not all 42.5 nm as in the 3-D case. Instead, if a 3-D insulation is sliced with a plane, the sliced insulation in the 2-D geometry will be $42.5/\sin(\cos^{-1}(\mathbf{n}_1 \cdot \mathbf{n}_2))$ nm, where $\mathbf{n}_1$ and $\mathbf{n}_2$ are the unit normals of the 3-D insulation and the plane that is slicing it.

Computing the effective *B-H* curves, we find the results depicted in Fig. 4b. We see that the computed *B-H* curves do not agree with the measured one and thus with the computational curves obtained by the 3-D model in the unsaturated region. There are various reasons for this. First, as Cyr et al. speculate, the missing 3-D flux paths could contribute to the lower initial permeability [4]. On the other hand, the insulations in the sliced 2-D geometries tend to be thicker than in the 3-D model, which could contribute to the lower initial permeability, as demonstrated by Vesa et al. [14]. Thirdly, the shapes of the insulations may also contribute to the unsaturated parts of the computational *B-H* curves, as suggested by Vesa et al. [17]. Since there is no symmetry that justifies the 2-D model, the results are expected. We note that a similar result was obtained by Sato et al. [12], in which the comparison was not carried out using 2-D slices of the 3-D geometries but a separately defined 2-D model.

The computational curves more or less agree with the measured one in the saturated region. This is due to the agreements of the volume fill fractions of the magnetizing matter in the 2-D slices and in the 3-D geometries. A visualization of a computational *B* field can be found in Fig. 5b.

4.3. Magnetostatic 2-D problem, field perpendicular to the plane

Let us now assume that in the 200 sliced 2-D geometries, much like the one depicted in Fig. 2, the magnetic field passes the plane perpendicularly. A uniform H_{eff} is defined on the plane and scaled into *B* using the material relation μ_0 in Ω_{nc} and the nonlinear *B-H* relation, 'Estimated local', depicted in Fig. 4a in Ω_{c}. Finally, the effective B_{eff} is computed by averaging the *B*-field over the plane.

In Fig. 4c, we see a comparison between the measured *B-H* curve and the computed 200 curves with the field perpendicular to the plane. We see that the computed *B-H* curves overshoot in the unsaturated region. The trend is easily explained by considering the 3-D extrusion of the 2-D geometry, depicted in Fig. 2, and considering the magnetic field traversing in the direction of the extrusion. There are no insulations to be passed, and hence the effective permeability is expected to be higher than in the 3-D case. We conclude that the 2-D model in this case is inconsistent with the 3-D model. This behavior is expected, since the 2-D model is not justified by any symmetry. On the other hand, the saturated parts of the computational curves, depicted in Fig. 4c, more or less agree with the measured one and hence with the curves obtained by the 3-D model, depicted in Fig. 4a. This is due to the volume fill fractions of the 2-D geometries being close to the volume fill fraction of the 3-D geometries.

4.4. Magnetostatic 3-D and 2-D problems in periodic setting

Let us now repeat the problems, described in Sections 4.1–4.3, but this time using periodic geometries. Fig. 6 visualizes a periodic geometry and its cross sectional slice. We assume that the edges of the geometries are scaled again to $l = 425$ μm, where l is given as in Fig. 3. The particles are insulated by 42.5 nm insulations once again. The formulations given in Sections 4.1–4.3 are applied, and the same localized *B-H* curve,

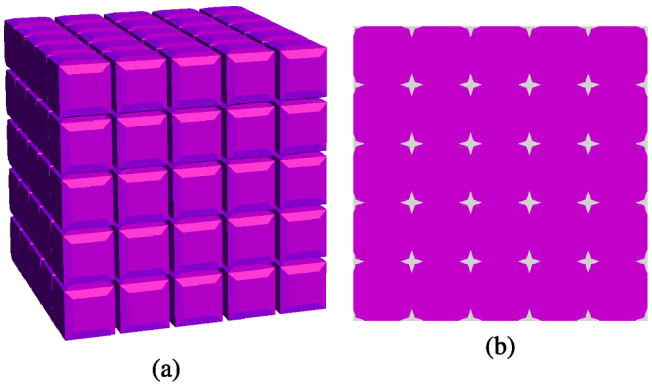

Fig. 6. Periodic geometries. (a) 3-D, (b) A 2-D slice of the 3-D geometry.

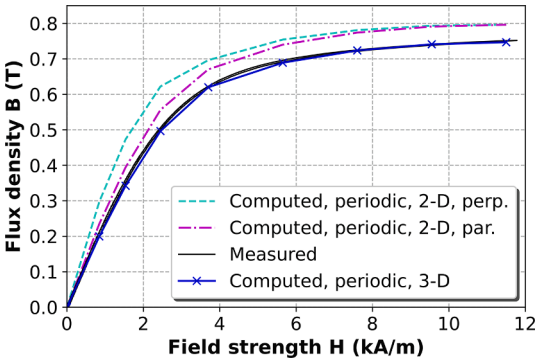

Fig. 7. A comparison of 3-D and 2-D models using periodic geometries. Nonlinear static *B–H* curves.

depicted in Fig. 4a, is used for the particles.

Fig. 7 depicts the computed *B-H* curves for each case: the 3-D model, the 2-D model with the field parallel to the plane, and the 2-D model with the field perpendicular to the plane. The measured curve is also visualized once again.

We notice that the 3-D model provides results consistent with the measurements. This is because the localized permeability was estimated against the measurement using one randomized 3-D geometry, and in this case, the results with the periodic 3-D geometry seem to agree well with the results using the randomized geometries. Both 2-D models provide higher saturation than the 3-D model. This is due to the volume fill fraction of the sliced 2-D geometry being higher than the volume fill of the original 3-D geometry. The computational curve, obtained by the 2-D model with the field perpendicular to the plane, provides initial permeability and the unsaturated part of the *B-H* curve higher than the 3-D model. This trend is consistent with the former results obtained using the randomized geometries, and the result may be explained by the magnetic field not passing any insulations if the 2-D geometry is extruded in the direction of the magnetic field.

However, in this case the computational *B-H* curve obtained by the 2-D model with the magnetic field parallel to the plane also provides higher initial permeability and higher unsaturated part of the effective *B-H* curve than the 3-D model. This result may be understood in two ways. First, if the 2-D geometry, depicted in Fig. 6b, is extruded in the direction perpendicular to the plane, there will be a higher fraction of the particle surfaces sharing the 42.5 nm 'thin insulation' than in the 3-D case, depicted in Fig. 6a. Second, the higher volume fill fraction of the 2-D model may play a role at least in the region close to saturation.

We conclude that the results obtained using the 2-D models are largely inconsistent with the 3-D model. The result is understandable, since there is no symmetry justifying either of the 2-D models. Periodicity does not free us from these issues.

5. Dynamical models

In this section, we compare three problems with the same material models consisting of a complex permeability and a resistivity. We compare a dynamical 3-D problem in the frequency domain with two dynamical 2-D problems in the frequency domain.

5.1. Dynamical 3-D problem

Consider the 200 3-D geometries, much like the one depicted in Fig. 1b and in the schematic Fig. 3. We use a time-harmonic $\mathbf{T}-\varphi$ formulation. The equations in the conductive magnetizing particles Ω_c, are given by

$$\begin{aligned} \nabla\times\left(\rho\nabla\times\underline{\mathbf{T}}\right) &= -\underline{j}\omega\underline{\mu}_r\mu_0\left(\underline{\mathbf{T}}-\nabla\underline{\varphi}\right), \\ \nabla\cdot\underline{\mu}_r\mu_0\left(\underline{\mathbf{T}}-\nabla\underline{\varphi}\right) &= 0, \end{aligned} \tag{3}$$

where the underlinings represent complex valued quantities. We set $\underline{\mathbf{T}} = 0$ in Ω_{nc} and in $\partial\Omega_c$. The material parameters ρ and $\underline{\mu}_r$ are estimated such that computations and measurements, that are presented later, agree [15]. The resistivity $\rho \approx 1.085\cdot10^{-7}$ Ωm. The complex relative permeability $\underline{\mu}_r \approx 306.17/\underline{-0.012}$, where the angle is in radians. Furthermore, in Ω_{nc},

$$\nabla\cdot\left(\mu_0\nabla\underline{\varphi}\right) = 0. \tag{4}$$

For $\underline{\varphi}$, we define boundary conditions on Γ_1 and Γ_2. First, $\underline{\varphi} = 0$ on Γ_1. Second, $\underline{\varphi} = \underline{H}_{\text{eff}}l$, which imposes sinusoidally pulsating magnetomotive forces of $\underline{H}_{\text{eff}}l$ for paths connecting the regions Γ_1 and Γ_2, provided that the paths do not enter inside the conductive particles. The $\underline{H}_{\text{eff}}$ is a chosen excitation, which will be discussed later.

The Eqs. (3) and (4) are discretized with the Galerkin method using a nodal scalar basis for φ and an edge basis for $\mathbf{T}$. The vector potential $\mathbf{T}$ is gauged in a spanning tree in Ω_c. From the field solutions, the effective *B*-field is computed by

$$\underline{B}_{\text{eff}} = \frac{1}{\text{Vol}}\int_\Omega \underline{\mathbf{B}}\cdot\mathbf{e}_1. \tag{5}$$

Due to linearity, we may easily set the magnitude of $\underline{B}_{\text{eff}}$ to the measured value 0.05 T (peak), that was held constant throughout the frequency sweep measurement. We set the excitation first to $\underline{H}_{\text{eff}} = 1$ (A/m), and then we scale the finite element solution accordingly, such that the magnitude of $\underline{B}_{\text{eff}}$ is 0.05 T.

From the field solutions, we may compute the loss density arising from current densities in resistive media from

$$w_{\text{ed}} = \text{Re}\left\{\frac{1}{\text{Vol}}\frac{1}{f}\int_{\Omega_c}\frac{1}{2}\overline{\underline{\mathbf{J}}}\cdot\rho\underline{\mathbf{J}}\right\}, \tag{6}$$

and the loss density arising from the changes in the magnetic field from

$$w_{\text{hy}} = \text{Re}\left\{\frac{1}{\text{Vol}}\int_{\Omega_c}\overline{\underline{\mathbf{H}}}\cdot\pi\underline{j}\underline{\mathbf{B}}\right\}. \tag{7}$$

We acknowledge the derivation by Ren et al. of a similar kind of loss formula [10]. It is expected that classical eddy current losses appear in (6) and hysteresis losses appear in (7). There is also a third loss mechanism, excess losses, explained in depth by Bertotti [18]. Since the terms (6) and (7) are the only terms, according to the Poynting theorem, contributing to losses in a magnetodynamical formulation, the excess losses can be found in these terms, provided that the material parameters have been properly identified.

Performing a computational frequency sweep for each of the 200 3-D geometries, we obtain the magnitudes of the dynamical relative permeabilities, depicted in Fig. 8 as '3-D'. The agreement with the measurements is good, since the material parameters of the computational

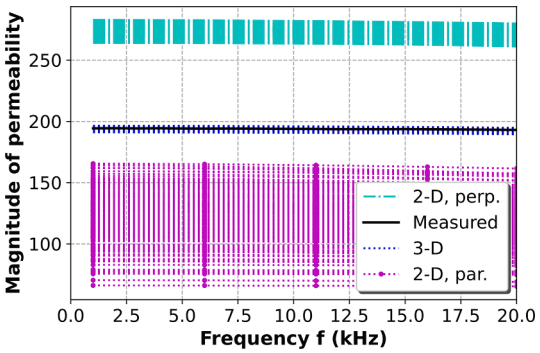

Fig. 8. Magnitudes of dynamical relative permeabilities. A comparison of 3-D and 2-D models.

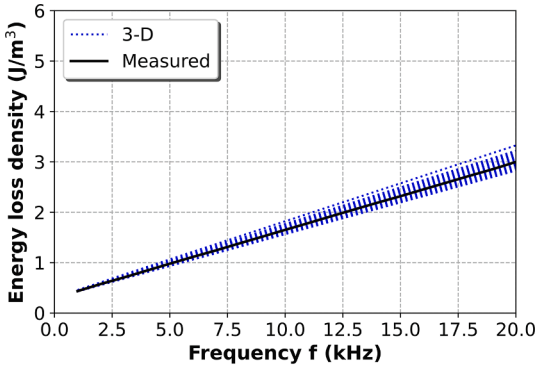

(a)

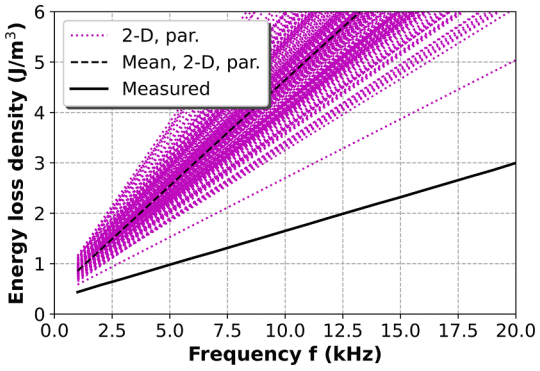

(b)

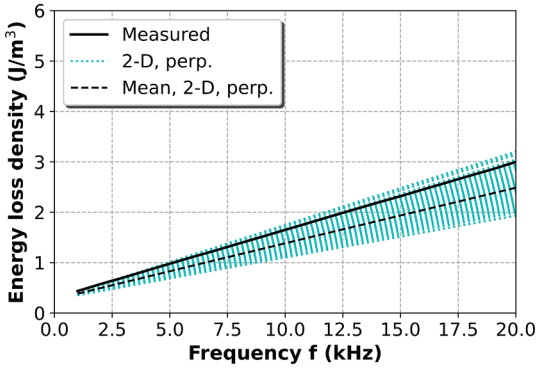

(c)

Fig. 9. Energy loss densities over one period of excitation. A comparison of 3-D and 2-D models.

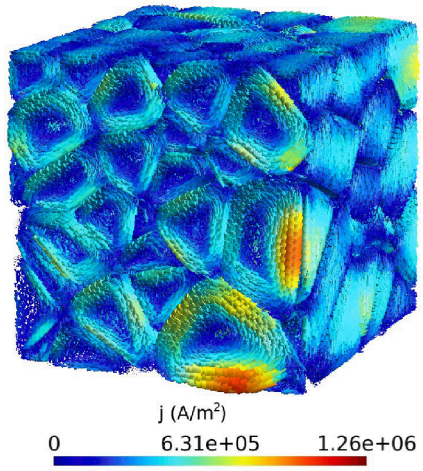

Fig. 10. A quarter-cycle capture of an eddy current field in 0.05 T 5 kHz excitation.

model were solved from an estimation problem. The measured and the computed losses are depicted in Fig. 9a. The losses agree due to the estimated nature of the material parameters. An eddy current field is visualized in Fig. 10.

5.2. *Dynamical 2-D problem with the magnetic field parallel to the plane*

Consider the 200 2-D geometries, much like the one depicted in Fig. 2, and in the schematic Fig. 3. The formulation, described in Section 5.1, is well-defined in 2-D, assuming that the eddy currents flow perpendicularly to the plane, but constrained in the sense that the net current in each particle is zero. We use the same material parameters as in the 3-D case in Section 5.1.

In Fig. 8, we see the computed magnitudes of the permeabilities, '2-D, par.', that agree neither with the 3-D results nor the measurements. The permeabilities are significantly lower. This is consistent with the nonlinear results showing lower permeabilities in the 2-D case. The reasons for such results were discussed in Section 4.2.

In Fig. 9b, we see the computed losses, '2-D, par.', and their mean, 'Mean, 2-D, par.'. The losses are significantly higher than in the 3-D case and in the measurements. To thoroughly explain the reasons for such results is a cumbersome task, but we must remember that the 2-D model assumes a translational symmetry in the direction perpendicular to the plane, and hence, the eddy currents flow without constraints in the geometry. Furthermore, the magnetic H-excitation is larger than in the 3-D case, since the amplitudes of B are matched to the measured value

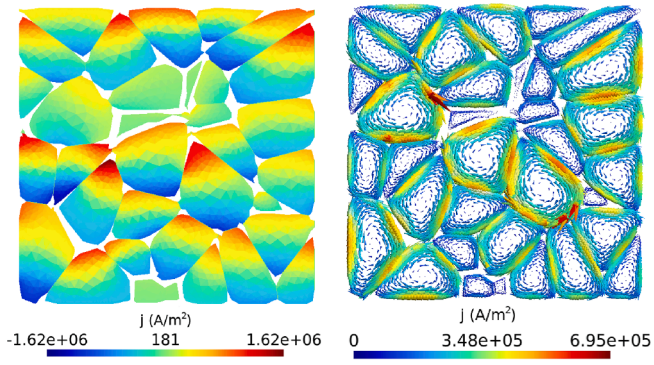

Fig. 11. A quarter-cycle capture of an eddy current field in 0.05 T 5 kHz excitation. (a) Magnetic field parallel to the plane. (b) Magnetic field perpendicular to the plane.

0.05 T. For these reasons, it is not surprising that the losses overshoot.

We conclude that the 2-D model with the magnetic field parallel to the plane and the eddy currents perpendicular to the plane is inconsistent with the 3-D model both permeability-wise and in terms of losses. It is no surprise, since no symmetry justifies such 2-D model. An eddy current field is visualized in Fig. 11a.

5.3. Dynamical 2-D problem with the magnetic field perpendicular to the plane

We consider again the 200 2-D geometries, much like the one depicted in Fig. 2 and in the schematic Fig. 3, but this time we assume that the magnetic field crosses the plane perpendicularly and the eddy currents circulate in each particle parallel to the plane. An H-formulation reads as

$$\nabla \times \rho \nabla \times \underline{\mathbf{H}} = -j\omega \underline{\mu}_r \mu_0 \underline{\mathbf{H}}, \tag{8}$$

where the material parameters are chosen to be the same as in the 3-D case in Section 5.1. The Eq. (8) was discretized with the Galerkin method using a nodal scalar (or a perpendicular edge if one wishes) basis for the magnetic field strength. A Dirichlet condition $\underline{\mathbf{H}} = H_{\text{eff}}\mathbf{e}_3$ was set in the nonconducting regions Ω_{nc} and in $\partial\Omega_{\text{c}}$, where $\mathbf{e}_3$ represents a unit vector, normal to the 2-D plane. The eddy currents are given by the curl of the magnetic field strength, and the $\underline{\mathbf{B}}$ field is obtained by a multiplication of the $\underline{\mathbf{H}}$ field by the permeability. An effective B field is given by

$$\underline{B}_{\text{eff}} = \frac{1}{\text{Vol}} \int_{\Omega} \underline{\mathbf{B}} \cdot \mathbf{e}_3, \tag{9}$$

which is just the average of the $\underline{\mathbf{B}}$ field over the surface of the domain. The magnetic H-excitation, determined by H_{eff}, was set to 1 (A/m), and due to the linearity of the problem, the FE-solution was scaled so that the magnitude of $\underline{B}_{\text{eff}}$ was matched with the measured 0.05 T. The formulas (6) and (7) for the loss densities are valid.

In Fig. 8, we see the computed magnitudes of the dynamical permeabilities, '2-D, perp.'. We notice that the permeabilities are significantly higher than in the 3-D case and in the measurements. The results are consistent with the nonlinear results, discussed in Section 4.3, and may be explained by the lacking of insulations to be passed by the magnetic field.

In Fig. 9c, we see the computed losses, '2-D, perp.', as well as their mean, 'Mean, 2-D, perp.'. The losses seem to almost agree with the measurements and thus with the results obtained from the 3-D model. This may be understood by the eddy currents being constrained inside the properly scaled particles mostly contributing to the losses. The underestimation of the losses may be due to the sliced particles having smaller radii than the original 3-D particles. Even though this result is somewhat positive, we must note that since the effective permeabilities of these 2-D models are significantly higher than the effective permeabilities of the 3-D models, the magnetic H-excitation is lower in the 2-D case than in the 3-D case in order to match the desired magnitude 0.05 T of $\underline{B}_{\text{eff}}$. Hence, the 2-D model is still inconsistent with the 3-D model even though the losses are close to agreeing. An eddy current field is visualized in Fig. 11b.

5.4. Magnetodynamic 3-D and 2-D problems in periodic setting

We repeat all three of the dynamical models, presented in Sections 5.1–5.3, but this time using the periodic geometries shown in Fig. 6. All the material parameters were chosen to be the same as in the 3-D model, presented in Section 5.1.

In Fig. 12a, we see a comparison of the computed and measured magnitudes of the relative effective permeabilities. The 3-D case provides the best match with the measurements since the material parameters used are of estimated nature. However, in the 2-D cases the

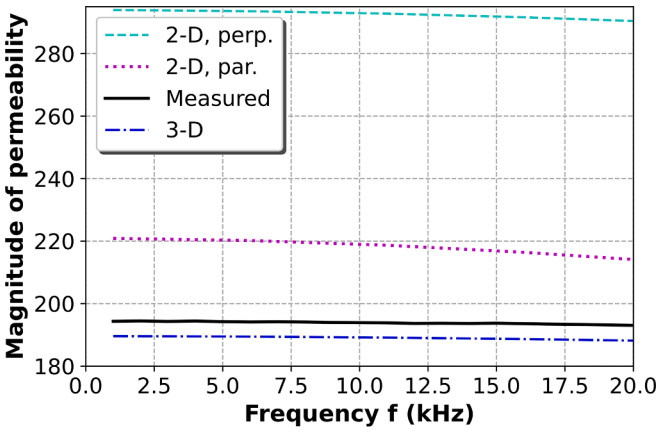

(a)

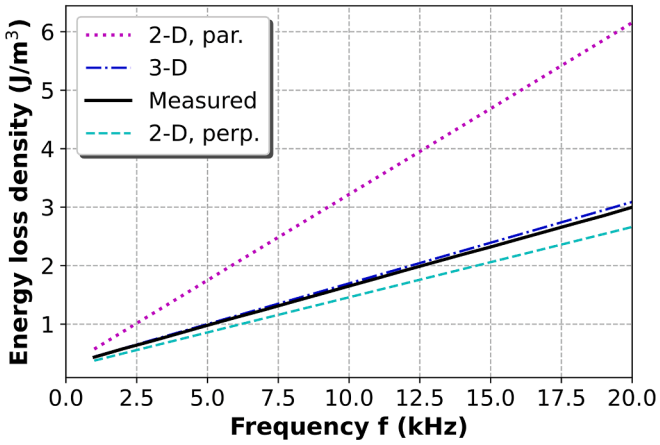

(b)

Fig. 12. A comparison of 3-D and 2-D models using periodic geometries. (a) Magnitudes of dynamical relative permeabilities. (b) Energy loss densities over one period of excitation.

permeabilities are higher. This is consistent with the nonlinear results discussed in Section 4.4.

In Fig. 12b, we see a comparison of losses obtained using the 3-D and 2-D models. Consistently with the results using the randomized 3-D geometries in Section 5.1, the periodic 3-D model provides losses that agree well with the measurements. This is again due to the estimated nature of the material parameters. The losses obtained by the 2-D model with the magnetic field parallel to the plane and the eddy currents perpendicular to the plane are significantly higher than in the 3-D case and thus the measurements. The results may be understood by the reasoning that was given in Section 5.2 for the corresponding models using the randomized 2-D geometries. The model using the periodic 2-D geometry with the field perpendicular to the plane and the eddy currents parallel to the plane seems to agree with the 3-D model. The result is still not consistent with the 3-D model, since the effective permeability in the 2-D case is significantly higher than in the 3-D case. We conclude that the 2-D models in the periodic setting are largely inconsistent with the 3-D model. This result is not a surprise, since there is no symmetry justifying the 2-D assumption.

5.5. Magnetodynamic 3-D and 2-D problems with rotating excitations

Next, we compare the losses provided by a 3-D and a 2-D model with rotating magnetic fields. A 3-D formulation is suitable for such problems. However, only such 2-D formulation is available, in which the

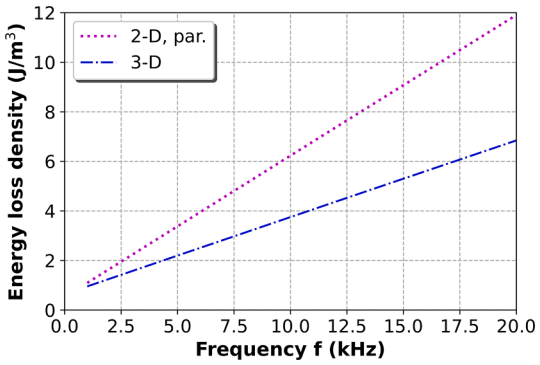

Fig. 13. A comparison of 3-D and 2-D models using periodic geometries with rotating magnetic excitations of 0.05 T.

magnetic field is rotating on the plane.

The formulations are again $T-\varphi$, as described in (3) and (4), and the losses are computed from (6) and (7). But this time the magnetic field is decomposed as $\underline{\mathbf{H}} = \underline{\mathbf{T}} - \nabla\underline{\varphi} + \underline{\mathbf{H}}_s$, where $\underline{\mathbf{T}} = 0$ on $\partial\Omega_c$, in Ω_{nc} and in the gauge tree of Ω_c, and $\underline{\varphi} = 0$ on $\partial\Omega$. The field $\underline{\mathbf{H}}_s$ is spatially constant and it is chosen so that an averaged magnetic flux density, as described in (5), corresponds to two sinusoidally pulsating 0.05 T flux densities in the directions of the basis vectors $\mathbf{e}_1$ and $\mathbf{e}_2$ with a $\pi/2$ phase difference.

For simplicity, the computations are carried out using just periodic 3·3·3- and 3·3-particle arrays, much like the 5·5·5- and 5·5-particle arrays depicted in Fig. 6. Fig. 13 visualizes the computed losses in the two cases: 2-D and 3-D. The results are showing large discrepancies. The losses obtained by the 2-D model are higher. Similar tendency was described and discussed in Sections 5.2 and 5.4. We conclude that similarly to the case of the magnetic field pulsating in one direction, the use of 2-D models with rotating fields is questionable due to the results being inconsistent with the 3-D model. This is not surprising, since no symmetry justifies the 2-D model.

6. Concluding remarks

In this article, we compared a 3-D model of an SMC material in a nonlinear static setting with two 2-D models. The 2-D geometries were cross-sectional slices of 3-D geometries. One of the 2-D models assumed that the magnetic field is parallel to the plane, and the other one of the 2-D models assumed that the magnetic field is perpendicular to the plane. It was found that in the unsaturated region the 2-D model with the magnetic field parallel to the plane underestimated the *B-H* curve. On the other hand, the 2-D model that assumed the magnetic field to be perpendicular to the plane overestimated the unsaturated part of the *B-H* curve. Reasons for such results were discussed. Considering periodic geometries, we found out that the result of one of the 2-D models overestimating the unsaturated part of the *B-H* curve and the other underestimating, is not a general tendency. However, consistency between the 2-D models and the 3-D model was not found. We conclude that the use of nonlinear static 2-D models of SMC materials is questionable if there is no symmetry in the geometry justifying such an assumption.

We also compared a 3-D model of an SMC material in a dynamical setting in frequency domain with two 2-D models. The 2-D geometries were cross-sectional slices of 3-D geometries. One of the 2-D models assumed that the magnetic field is parallel to the plane, and the eddy currents are perpendicular to the plane. The other of the 2-D models assumed vice versa. The results for the computed dynamical effective permeabilities showed similar results to the nonlinear setting, the 2-D models being inconsistent with the 3-D model. On the other hand, a comparison of the losses showed that the 2-D model that assumed the magnetic field to be parallel to the plane and the eddy currents perpendicular to the plane overestimated losses. Reasons for such a result were discussed. In terms of losses, the results were similar if the magnetic field was rotating instead of pulsating in one direction. The 2-D model that assumed the magnetic field to be perpendicular to the plane and the eddy currents parallel to the plane provided almost consistent losses with the 3-D model, but these losses were slightly smaller. The 2-D model was still inconsistent with the 3-D model in terms of permeability. The same tendency for losses was present when using periodic geometries.

The proposal of this article is to be very critical towards 2-D models of SMC materials if there is no symmetry in the 3-D geometry that justifies the 2-D model. Periodicity is not such a justification.

CRediT authorship contribution statement

J. Vesa: Conceptualization, Methodology, Software, Formal analysis, Investigation, Writing, Visualization. **P. Rasilo:** Conceptualization, Methodology, Supervision, Project administration, Funding acquisition.

Declaration of Competing Interest

The authors declare that they have no known competing financial interests or personal relationships that could have appeared to influence the work reported in this paper.

Acknowledgement

The foundation of Emil Aaltonen and the Academy of Finland (grant agreement No 307675) are acknowledged for financial support. J. Vesa thanks Saara Göös for reading the paper and commenting on the style. This project has received funding from the European Research Council (ERC) under the European Union's Horizon 2020 research and innovation programme (grant agreement No 848590).

References

[1] H. Shokrollahi, K. Janghorban, Soft magnetic composite materials (SMCs), Journal of Materials Processing Technology 189 (Feb. 2007).
[2] H. Waki, H. Igarashi, T. Honma, Estimation of Effective Permeability of Magnetic Composite Materials, IEEE Transactions on Magnetics 41 (5) (2005).
[3] O. Bottauscio, M. Chiampi, A. Manzin, Homogenized magnetic properties of heterogeneous anisotropic structures including nonlinear media, IEEE Transactions on Magnetics 45 (10) (2010).
[4] C. Cyr, P. Viarouge, S. Clénet, J. Cros, Homogenized magnetic properties of heterogeneous anisotropic structures including nonlinear media, IEEE Transactions on Magnetics 45 (10) (2010).
[5] A. Bordianu, O. de la Barrière, O. Bottauscio, M. Chiampi, A. Manzin, A multiscale approach to predict classical losses in soft magnetic composites, IEEE Transactions on Magnetics 48 (4) (2012).
[6] T. Henneron, A. Benabou, S. Clénet, Nonlinear proper generalized decomposition method applied to the magnetic simulation of a SMC microstructure, IEEE Transactions on Magnetics 48 (11) (2012).
[7] X. Ren, R. Corcolle, L. Daniel, A. The, 2D finite element study on the role of material properties on eddy current losses in soft magnetic composites, European Physical Journal Applied Physics 73 (2016).
[8] Y. Ito, H. Igarashi, M. Suzuki, Y. Iwasaki, K. Kawano, Effect of magnetic contact on macroscopic permeability of soft magnetic composite, IEEE Transactions on Magnetics 52 (3) (2016).
[9] X. Ren, R. Corcolle, L. Daniel, Losses approximation for soft magnetic composites based on a homogenized equivalent conductivity, Advanced Electromagnetics 5 (2) (2016).
[10] X. Ren, R. Corcolle, L. Daniel, A homogenization technique to calculate eddy current losses in soft magnetic composites using a complex magnetic permeability, IEEE Transactions on Magnetics 52 (12) (2016).
[11] A. Maruo, H. Igarashi, Analysis of magnetic properties of soft magnetic composite using discrete element method, IEEE Transactions on Magnetics 55 (6) (2019).
[12] H. Sato, A. Maruo, H. Igarashi, Analysis of nonlinear magnetic properties of soft magnetic composite using 2d and 3d discrete element methods, International Journal of Applied Electromagnetics and Mechanics, Early Access, 2020.
[13] J. Vesa, P. Rasilo, Producing 3-d imitations of soft magnetic composite material geometries, IEEE Transactions on Magnetics 55 (10) (2019).

[14] J. Vesa, P. Rasilo, Permeability estimations of SMC material particles, IEEE Transactions on Magnetics 56 (9) (2020).
[15] J. Vesa, P. Rasilo, Permeability and resistivity estimations of SMC material particles from eddy current simulations, Journal of Magnetic Materials (2020). Accepted.
[16] Magnetics Inc. C055106A2 datasheet, Revision Nov. 2016, https://www.mag-inc.com/Media/Magnetics/Datasheets/C055106A2.pdf.
[17] J. Vesa, T. Karhula, A. Marjamäki, J. Panchal, P. Rasilo, Mimicking soft magnetic composite geometries algorithmically, International Journal of Applied Electromagnetics and Mechanics 59 (1) (2019).
[18] G. Bertotti, General properties of power losses in soft ferromagnetic materials, IEEE Transactions on Magnetics 24 (1) (1988).